Marine Structures 75 (2021) 102813

Contents lists available at ScienceDirect

Marine Structures

journal homepage: http://www.elsevier.com/locate/marstruc

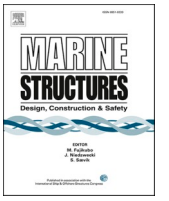

A procedure for predicting the permanent rotation of monopiles in sand supporting offshore wind turbines

Ana M. Page *, Rasmus Tofte Klinkvort, Steven Bayton, Youhu Zhang, Hans Petter Jostad

Norwegian Geotechnical Institute (NGI), Oslo, Norway

ARTICLE INFO

Keywords:
Offshore wind turbine foundations
Design
Serviceability limit state
Accumulated rotation
Numerical modelling
High cycle accumulation

ABSTRACT

Foundations for Offshore Wind Turbines (OWTs) are designed following the limit state philosophy. One of the considered states is the Serviceability Limit State (SLS), which verifies that the permanent rotation of the foundation generated from accumulated strains in the soil is below a project specific criterion. Despite design codes requiring an estimation of the permanent rotation, there is not clear guidance on how to implement this. This paper describes a methodology to estimate the monopile permanent rotation for SLS and discusses its advantages and limitations. The methodology combines an accumulation method with results from 3D Finite Element Analyses (FEA) and a soil model that accounts for strain accumulation as a function of the number of cycles, relative density and load characteristics. The performance of the proposed methodology is compared against experimental centrifuge tests and results from advanced 3D FEA, indicating that it can predict the permanent rotation with satisfactory accuracy, and with a considerable reduction in computational effort. This is important for the design of OWTs, where different load histories might be required to be checked – often under tight time constraints – to find which load history leads to the largest permanent rotation, and therefore is more critical to SLS design.

1. Introduction

Offshore wind energy is experiencing one of the fastest growth rates of all renewable energy sources [1]. Although the cost of offshore wind energy has decreased dramatically in recent years [2], further cost reduction can be achieved. Improving the accuracy of the tools used in the design process can reduce uncertainties and risks, leading to more cost-efficient designs.

Offshore Wind Turbines (OWTs) are designed following the limit state philosophy. One of the considered states is the Serviceability Limit State (SLS), which deals with the appropriate operation and appearance of the structure. For monopiles, the SLS requires verification that the permanent rotation of the foundation at the end of lifetime is below a project specific criterion. Despite codes and design guidelines indicating how to estimate loads on OWTs, there is no guidance nor consensus on an accepted methodology to estimate the accumulated or the permanent rotation.

OWTs are continuously subjected to cyclic loads from the offshore environment, and during its lifetime, typically 25–30 years, monopiles are exposed to millions of load cycles. Cyclic loads are transferred to the soil surrounding the monopile as cyclic stresses, which may lead to a complex combination of changes in soil density, accumulation of pore pressures and redistribution of sand grains

* Corresponding author.
E-mail address: ana.page@ngi.no (A.M. Page).

https://doi.org/10.1016/j.marstruc.2020.102813
Received 30 July 2019; Received in revised form 28 April 2020; Accepted 24 June 2020
Available online 25 September 2020

[3], resulting in an accumulation of pile rotation. Some methods for predicting the accumulation of displacement and rotation of monopiles exist, and most of these can be classified either as semi-empirical or as numerical approaches. In the semi-empirical approaches, the accumulated rotation observed in experimental tests is used to calibrate simple models that predict the accumulated rotation as a function of the number of cycles and the load characteristics. The numerical approaches link the soil response, computed in terms of accumulated soil strains and redistribution of effectives stresses, to the accumulated pile head displacement and rotation.

Semi-empirical models are often based on results from: field tests, 1g model tests and centrifuge model tests. Table 1 provides an overview of pile tests that have been employed to derive simple semi-empirical models. In most of the existing semi-empirical equations, the relation between the accumulated displacement or rotation and the number of cycles follows a power law, a logarithmic law or a logarithmic-linear law [3]. Models based on a power law were originally proposed for long slender piles by Little and Briaud [4] and by Long and Vanneste [5], and for monopiles by LeBlanc et al. [6] and Klinkvort and Hededal [7] based on experimental results with a maximum number of cycles between 50 and $6.5 \cdot 10^4$. Logarithmic accumulation laws have been proposed by for example by Lin and Liao [8] and Verdure et al. [9] for slender piles and by Peralta and Achmus [10] and Li et al. [11] for monopiles, based on tests subjected up to a maximum of 10^4 cycles. Peralta and Achmus [10] highlight that accumulated displacement from experimental results in flexible piles is best described by a logarithmic law, while the results from monopiles are better described by a power law. In addition, logarithmic-linear expressions have recently been proposed by Dührkop [12] and by Bienen et al. [13] for monopiles. This law represents well the accumulation of displacements seen in the tests from Cuéllar [3], where $5 \cdot 10^6$ cycles have been applied to a model monopile.

A weakness of these semi-empirical models is that they are typically derived for a specific set of conditions (geometry, loads and soil), and it can therefore be difficult to extrapolate the methods to sites with different soil and load conditions. In addition, the number of cycles applied in the experimental tests are generally below the number of cycles expected during the lifetime of a monopile. This implies that these models often have to be extrapolated outside their validation range if they were to be applied in practice.

As an alternative to semi-empirical expressions, various numerical approaches have been proposed. These approaches share the similarity that the response of monopiles to long-term cyclic loading, and more specifically the accumulated rotation, can be computed based on soil behaviours measured at element level. One of the most common numerical approaches is Finite Element Analyses (FEA) in combination with explicit constitutive models that can account for the accumulation of strains as a function of the number of cycles, relative density and load characteristics. For instance Jostad et al. [14], presented a procedure to calculate the effect of cyclic loading in FEA for loading conditions where significant generation of pore pressures is expected. The procedure is based on undrained soil element test results and the effect of drainage is taken into account by performing the analyses by a fully coupled consolidation formulation. Lesny et al. [15] and Achmus et al. [16] proposed methodologies to transfer the results from cyclic drained triaxial element tests to FEA based on a reduction of the elastic modulus of the soil. In particular, Achmus et al. [16] suggested to reduce the constrained elastic modulus as a function of the number of cycles and the loading amplitude. The method by Achmus et al. [16] has been compared with the single amplitude small-scale tests from Peralta and Achmus [10] and Hettler [17], and it provides good agreement for single amplitude load histories. However, there is no indication on how it can be applied to multi-amplitude load histories. Another explicit constitutive model is the High Cycle Accumulation (HCA) model from Niemunis et al. [18], which predicts the accumulated strain as a function of the number of cycles, loading characteristics, relative density and effective stresses. The HCA accumulation model has been validated, at element level, against cyclic triaxial texts [19], and at foundation level, by comparing numerical simulations against small-scale and large-scale tests [20–22]; providing good agreement for both single- and multi-amplitude tests.

The advantage of using a numerical approach based on 3D FEA is that the input can be derived from laboratory tests, which allows the model to be used for varying and more realistic site conditions. The main disadvantage is that 3D FEA is time-consuming, especially when different load histories have to be evaluated. This is important for the design OWT, where several combinations of time load series and occurrences might be checked – often under tight time constraints – to find which load combinations lead to the largest permanent rotation, and therefore are more critical to the SLS.

Table 1
Overview of cyclic lateral load tests on piles in sand evaluating the accumulation of displacement and rotation.

Reference	Test type	Load packets	Max. number of cycles	L/D ratio[a]
Little and Briaud [4]	Full scale	Single amplitude	20	32.0–60.0
Long and Vanneste [5]	Full scale	Single amplitude	50	12.7
Li et al. [23]	Large scale	Multi-amplitude	5000	6.5
Peralta and Achmus [10]	Small scale (1*g*)	Single amplitude	10 000	4.8–6.7
LeBlanc et al. [6]	Small scale (1*g*)	Single amplitude	65 000	4.5
LeBlanc et al. [24]	Small scale (1*g*)	Multi-amplitude	10 100	4.5
Cuéllar [3]	Small scale (1*g*)	Single amplitude	5 000 000	4.0
Verdure et al. [9]	Centrifuge (40*g*)	Single amplitude	50	16.7
Bienen et al. [13]	Centrifuge (200*g*)	Single amplitude	1000	4.0–12.5
Klinkvort and Hededal [7]	Centrifuge (75*g*)	Single amplitude	10 000	6.0
Rudolph et al. [25]	Centrifuge (200*g*)	Single amplitude	13 000	5.0
Bayton et al. [26]	Centrifuge (100*g*)	Multi-amplitude	96 000	5.0
Truong et al. [27]	Centrifuge (250*g*)	Multi-amplitude	1500	6–11.4

[a] Typical length-to-diameter L/D ratios for monopiles supporting OWTs range between 2.5 and 6.

This paper describes a design methodology to compute the monopile permanent rotation for the SLS. The methodology combines results from 3D FEA with the HCA model – which accounts for the accumulation of strains as a function of the number of cycles, relative density and load characteristics – with an accumulation method. It benefits from the accuracy from 3D FEA at the computational speed of the simpler methods, as it allows for variations of the load histories without having to repeat computationally expensive FEA. The paper is structured as follows. Section 2 describes the proposed methodology and its calibration. Section 3 then demonstrates how to employ this methodology, and presents the verification against more advanced 3D FEA. This is followed by Section 4, which compares the accumulated rotation predicted with the proposed methodology against results from centrifuge tests. Finally, Section 5 discusses the results, highlighting the advantages and limitations, and Section 6 outlines the conclusions.

2. Proposed methodology for predicting the permanent rotation of monopiles

2.1. Overview

The proposed methodology predicts the permanent rotation of monopiles by combining results from 3D FEA – presented as contour diagrams – with an accumulation procedure where the load history is applied as packets of regular cycles with constant cyclic loads and periods. Fig. 1 displays an overview of the steps included in the proposed methodology and the order in which they are executed. Note that the permanent rotation includes both the accumulated rotation – which depends on the number of cycles – as well as the rotation generated from changes in the average and cyclic loads.

The accumulation procedure employed in the proposed methodology is similar to the NGI accumulation procedure [28], but instead of employing the soil's cyclic strain as memory of the effects of cyclic loading, it uses the monopile permanent rotation at seafloor. The idea of employing the rotation as state variable has been recently presented in Bayton et al. [26] for computing the permanent rotation from centrifuge tests. However, in the current proposed approach, the rotation contour diagrams are not derived from model tests, which might be impractical in the design of OWTs, but computed from constant-amplitude 3D FEA with the HCA model. In this manner, the proposed procedure combines the benefits from FEA with a constitutive model that can account for the accumulation of strains as a function of the number of cycles, relative density and load characteristics with a simple and robust accumulation procedure. In addition, the input parameters describing the strain accumulation in the soil can be obtained from cyclic soil element laboratory tests, alone, or in combination with correlations from the literature [29]; which makes the methodology more suitable to OWT design. Once the rotation contour diagrams are established, this procedure can be employed to compute the permanent monopile rotation for different combinations of load time histories.

2.2. Load histories

In nearly all of the existing methods for predicting the accumulated rotation, the irregular load time histories are not applied as such, but they are first simplified to regular cyclic load packets, each with a constant average component M_{av}, a constant cyclic amplitude M_{ampl} and a constant period. The transformation from irregular load time histories to sorted load packets can be performed by e.g. rainflow counting [30] or other cycle counting methods [31]. Fig. 2 plots a snapshot of time of a simulated moment load at seafloor from a ULS storm acting on a 10 MW monopile-based OWT, and the corresponding sorted load history in packets by rainflow counting.

Traditionally, cycle counting methods have arranged the idealised load histories as packets of equal cyclic loading amplitude M_{ampl} and equal average component M_{av}. However, due to the impact of the $M_{max} = |M_{av} + 1/2 \cdot M_{ampl}|$ values and the $M_{min}/M_{max} = |M_{av} - 1/2 \cdot M_{ampl}|/|M_{av} + 1/2 \cdot M_{ampl}|$ ratio on the accumulated rotation, the regular cyclic load histories are often described by two

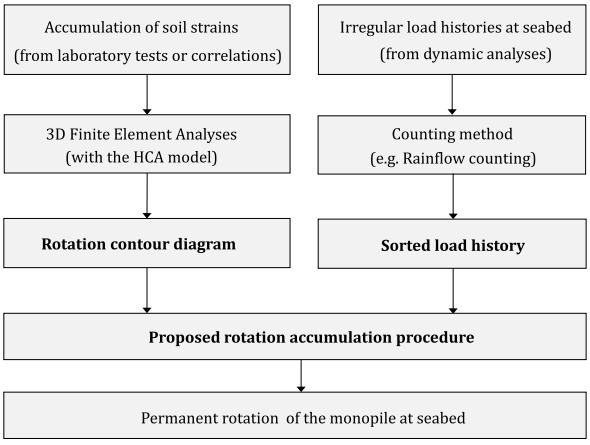

Fig. 1. Proposed methodology for predicting the permanent rotation of monopiles.

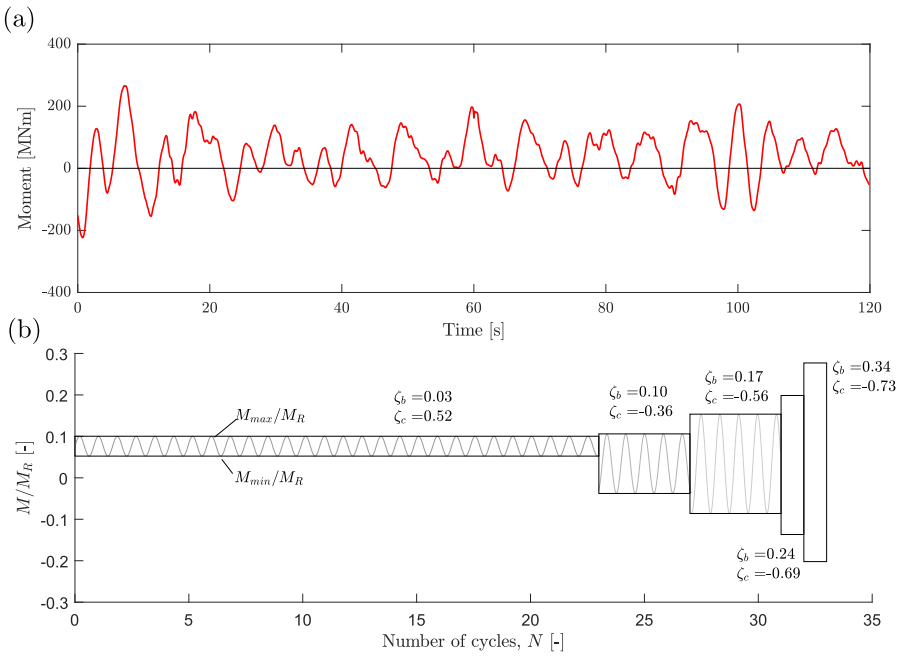

Fig. 2. Simulated moment load at seafloor from a ULS storm acting on a 10 MW monopile-based OWT: (a) Load history in the time domain; (b) Sorted load history by rainflow counting.

non-dimensional load ratios, defined as:

$$\zeta_b = \frac{M_{max}}{M_R} \quad \zeta_c = \frac{M_{min}}{M_{max}} \tag{1}$$

where M_R is a reference load value and M_{min} and M_{max} are the absolute minimum and maximum values of the regular cycles in each load packet, as illustrated in the first cyclic load packet displayed in Fig. 2b. The reference load value M_R can be defined following different criteria. Bayton et al. [26] define M_R as the monotonic moment at seabed that leads to a permanent rotation (i.e. after unload) equal to 0.25°. Another criterion is proposed by LeBlanc et al. [6], who defined M_R as the moment that causes a peak rotation equal to 4° – considered to represent the foundation failure. This paper follows the criterion proposed in Bayton et al. [26].

2.3. Contour diagrams

The rotation contour diagrams are derived from 3D FEA of the soil and the monopile, where single load-amplitudes – that is, constant ζ_b and ζ_c – are applied. An example of the construction of the rotation contour diagram is shown in Fig. 3. The contours displayed in Fig. 3 include both the accumulated rotation – generated from accumulation of strains in the soil around the monopile – as well as the rotation generated from changes in the average loads.

The accumulation of strains in the soil is computed in the 3D FEA by employing the HCA model described in Niemunis et al. [18]. In this explicit model, the rate of strain accumulation $d\varepsilon_{acc}$ is calculated, for each loading packet, as a function of the current average effective stresses, void ratio and an equivalent number of drained cycles of strain amplitude ε_{amp}. The rate of strain accumulated is given by a set of empirical functions as follows:

$$d\varepsilon_{acc} = f_{ampl}\dot{f}_N f_e f_p f_Y f_\pi \tag{2}$$

where f_{ampl} accounts for the effect of the cyclic strain amplitude, $\dot{f}_N$ the cyclic history by the equivalent number of drained cycles, f_e the effect of void ratio, f_p the effect of effective mean stress level, f_Y the effect of the average shear stress level, and f_N the effect of change polarisation of the cycles. Table 2 summarises these empirical functions. In the model implementation, the strain amplitude ε_{amp} is, for simplicity, calculated following degradation function proposed by Hardin and Drnevich [32]:

$$\frac{G}{G_{max}} = \frac{1}{1 + (\gamma_{cy}/\gamma_r)^\alpha} \tag{3}$$

where G is the secant shear modulus, G_{max} the small-strain shear modulus, γ_{cy} the cyclic shear strain amplitude, γ_r a reference shear strain, and α the curvature parameter. G_{max} is approximated with the expression proposed by Hardin and Black [33]:

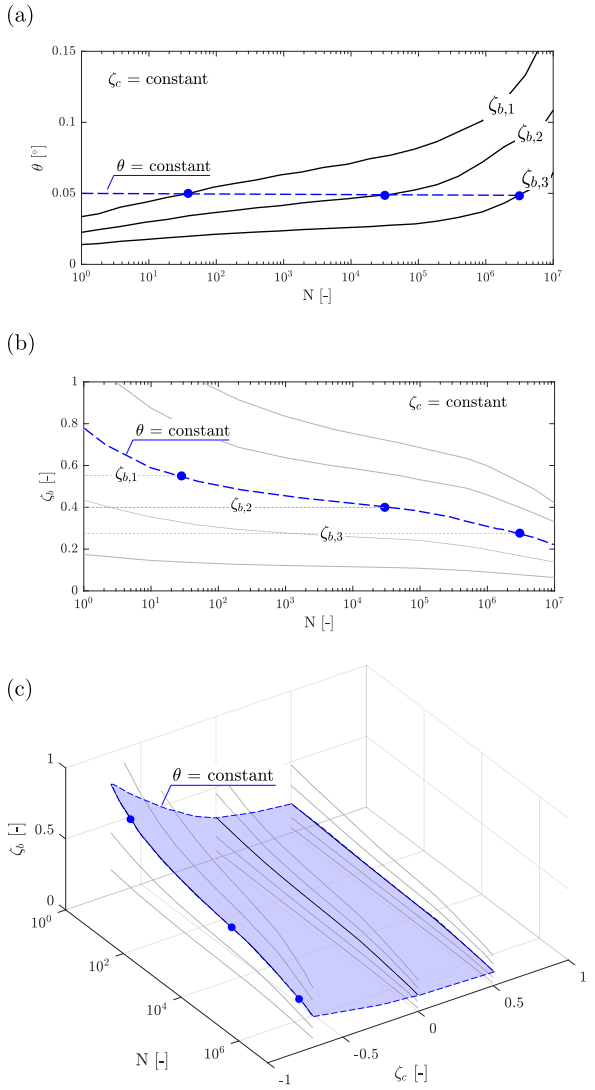

Fig. 3. Construction of the rotation contour diagram from FEA with the HCA model for different combinations of ζ_b and ζ_c: (a) FEA results for constant ζ_b and ζ_c; (b) Cross-section of a contour diagram for constant ζ_c; and (c) 3D contour diagram.

Table 2
Empirical functions employed in the HCA model to calculate of the rate of strain accumulation, after Niemunis et al. [18].

Influencing parameter	Function	Material constants
Strain amplitude	$f_{ampl} = \min[(\varepsilon^{amp}/10^{-4}); 10^{C_{amp}}]$	C_{amp}
Cyclic preloading	$\dot{f}_N = \dot{f}_N^A + \dot{f}_N^B$	
	$\dot{f}_N^A = C_{N1} C_{N2} \exp(-g^A/(C_{N1} f_{ampl}))$	C_{N1}, C_{N2}
	$\dot{f}_N^B = C_{N1} C_{N3}$	C_{N3}
Average mean pressure	$f_p = \exp\left[-C_p(p^{av}/p_{atm} - 1)\right]$	C_p
Average stress ratio	$f_Y = \exp(C_Y \overline{Y}^{av})$	C_Y
Void ratio	$f_e = \frac{(C_e - e)^2}{1+e} \frac{1+e_{max}}{(C_e - e_{max})^2}$	C_e

$$G_{max} = g_0 \frac{(e_g - e)^2}{1+e} \left(\frac{p}{p_{atm}}\right)^{n_g} p_{atm} \tag{4}$$

where e is the void ratio, p the mean stress, p_{atm} a reference stress and g_0, e_g and n_g are dimensionless material constants. Additionally, in the present HCA model, the changes in effective mean stress, p', and deviatoric stress, q, are computed as follows:

$$dp' = K(d\varepsilon_{vol} - d\varepsilon_{acc} m_{vol}); \quad dq = 3G\left(d\varepsilon_q - d\varepsilon_{acc} m_q\right) \tag{5}$$

where $d\varepsilon_{vol}$ and $d\varepsilon_q$ are the changes in volumetric and deviatoric strain, m_{vol} and m_q are the volumetric and deviatoric components of the normal vector to the modified Cam-Clay yield surface passing through the current stress point, and K is the stress dependent bulk modulus defined as:

$$K = B\left(\frac{p}{p_{atm}}\right)^n p_{atm} \tag{6}$$

where B and n are dimensionless material constants. For the calculation of stresses, the shear modulus G is derived from K following an elastic relation. For more details on the presented implementation of the HCA model, the reader is referred to Jostad et al. [34].

2.4. Accumulation procedure

A rotation accumulation procedure – based on the NGI accumulation procedure – is employed to predict the permanent rotation from contour diagrams (see for instance the contours from Fig. 3) for a series of load packets with different load characteristics ζ_b and ζ_c. It is based on the condition that the monopile rotation at seafloor at the start of a load packet is equal to the monopile rotation at the end of the previous load packet. This assumes that the soil state around the monopile (e.g. void ratio, accumulated strain, etc) is uniquely defined by the monopile rotation. The procedure is illustrated in Fig. 4 by means of an example that assumes the cyclic history listed in Table 3. In the first load packet, the monopile rotation starts at point A in the rotation contour diagram displayed in Fig. 4, which corresponds to 1 cycle at $\zeta_b = 0.2$ and $\zeta_c = 0$. After $8 \cdot 10^5$ cycles are applied, the permanent rotation is increased from the rotation at point A ($\theta = 0.02°$) to the rotation at point B ($\theta = 0.05°$). In the second load packet, the load characteristics are increased to $\zeta_b = 0.4$ and $\zeta_c = 0$. The monopile and soil system remembers the permanent rotation it had at the end of the previous load packet (at point B), and it will have this permanent rotation when the second loading packet starts. In Fig. 4b, this means that the monopile and soil system will follow the rotation contour from point B to the new loading characteristics, at point C. From the diagram it can be seen that the equivalent number of cycles at point C is close to 2. This means that applying $8 \cdot 10^5$ cycles at $\zeta_b = 0.2$ and $\zeta_c = 0$ is equivalent to applying 2 cycles at $\zeta_b = 0.4$ and $\zeta_c = 0$. The rotation generated in the second load packet will therefore be estimated from point C.

The permanent rotation in the second load packet is due to: (1) the change in load characteristics; and (2) the effect of the applied number of cycles. First, the change in the load characteristics – which is equivalent to a change in the average load acting on the monopile following the relation $\Delta M = \Delta(\zeta_b \cdot (1 + \zeta_c)/2) \cdot M_R$– leads to an instant change in rotation ($\Delta\theta$). Fig. 4a illustrates the change in rotation due to a change in the applied average load. Note that this change in rotation is independent of the number of cycles, and it can be estimated from the moment-rotation non-linear curve derived from a pushover analysis. The $\Delta\theta$ in Fig. 4a takes the monopile and soil system from point C to point D. Then, the effect of the applied number of cycles (10^4 cycles in the second load packet) brings the permanent rotation from the rotation at point D to the rotation at point E ($\theta = 0.20°$). Note that this procedure differs from the strain superposition or accumulation methods proposed by Stewart [35] for ballast or by Lin and Liao[8] for sands, since it adds the rotation generated after changes in the load characteristics.

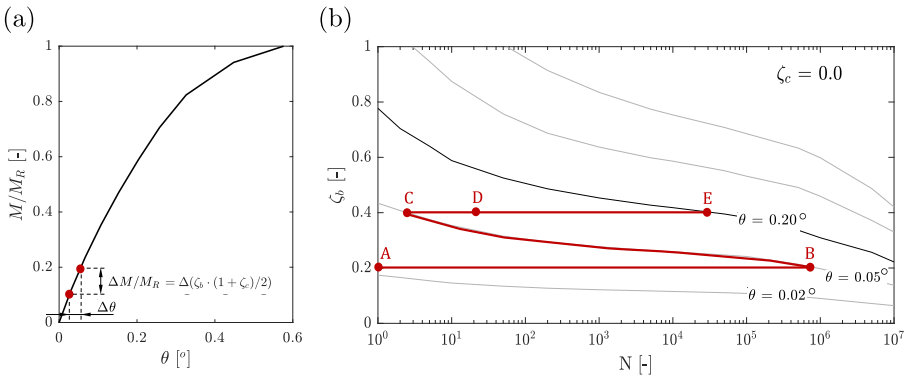

Fig. 4. Illustration of the rotation accumulation procedure: (a) moment - rotation curve employed to compute the instant change in rotation due to a change in the applied average load; and (b) accumulation path along the contours of permanent rotation.

Table 3
Sorted cyclic load history employed in the example illustrating the rotation accumulation procedure.

Number of cycles, N	ζ_b	ζ_c
$8 \cdot 10^5$	0.2	0.0
10^4	0.4	0.0

3. Performance of the proposed methodology

3.1. Overview

The performance of the proposed methodology is illustrated for a case study, and compared against results from 3D FEA simulations for a series of sorted load histories. The case study is based on the WAS-XL monopile in sand [36], a reference design for large diameter monopile foundations. The WAS-XL monopile was designed to support the DTU 10 MW OWT [37], and the pile dimensions and applied loads are considered to be representative for typical offshore wind sites [36]. Fig. 5 displays the overall dimensions and soil conditions of the case study OWT, which considers a Mean Sea Level (MSL) of 30 m. The commercial 3D FEA code PLAXIS [38] was employed to generate the contour diagrams and to perform the FEA used in the comparison. The accumulated strains in the soil volume were predicted with the implementation of the HCA model described in Jostad et al. [34].

3.2. Case study

3.2.1. Soil properties

The soil considered in the case study is a homogeneous sand profile of Karlsruhe fine sand, which is a well-documented sand from the literature [19]. A constant relative density of 62% was assumed. Table 4 lists the HCA model parameters for Karlsruhe fine sand – the calibration of which can be found in Wichtmann [19]– and Table 5 lists the model parameters employed in the estimation of the strain amplitude. The strain amplitude is calculated at each integration point by employing the modulus reduction curve from Hardin and Drnevich [32], displayed in Eq. (3). Following the approach presented in Wichtmann [19], the calibrated parameters in Table 5 represent the stress-strain curve that could be obtained in the second loading cycle, not the stress-strain curve representing the monotonic response.

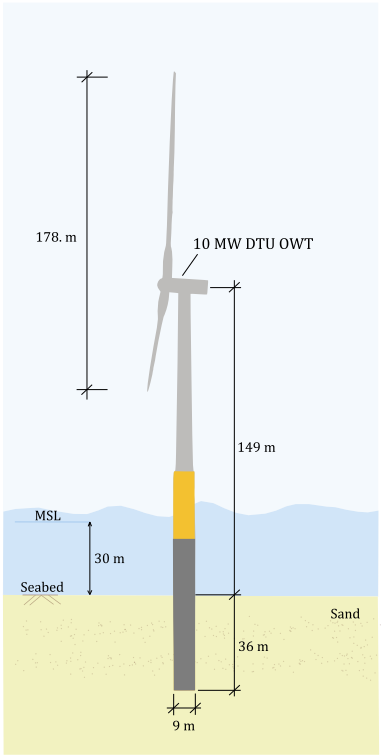

Fig. 5. Overview of the dimensions and soil conditions of the case study Offshore Wind Turbine (OWT).

Table 4
Dimensionless parameters of the HCA model for Karlsruhe fine sand, after [19].

C_{amp}	C_e	C_p	C_Y	C_{N1}	C_{N2}	C_{N3}
1.33	0.60	0.23	1.68	$2.95 \cdot 10^{-4}$	0.41	$1.90 \cdot 10^{-4}$

Table 5
Model parameters employed in the estimation of the strain amplitude for Karlsruhe fine sand from Eqs. (3), (4) and (6).

γ_r	α	g_0	e_g	n_g	B	n	p_{atm}
$8 \cdot 10^{-4}$	0.70	2000	1.6	0.5	435	0.5	100 kPa

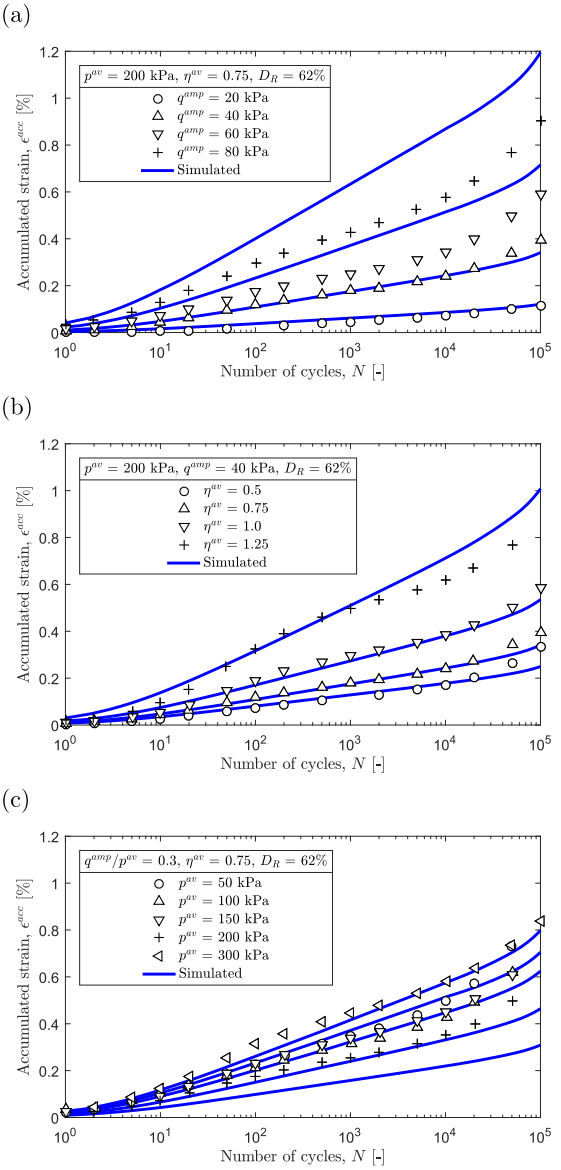

Fig. 6. Comparison between the experimental drained cyclic test results from Wichtmann [19] and simulations with the HCA model: (a) effect of the deviatoric stress amplitude q^{amp}; (b) effect of the average stress ratio $\eta^{av} = q^{av}/p^{av}$; and (c) effect of the effective mean stress p^{av}.

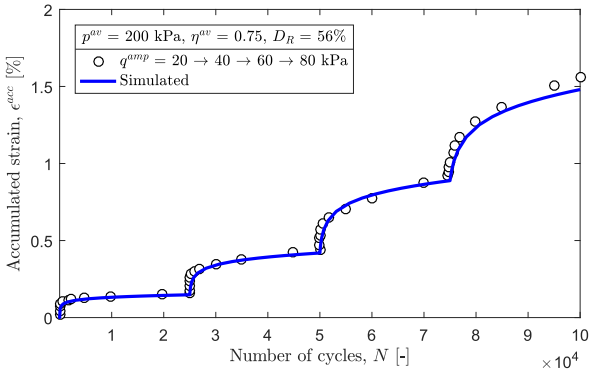

Fig. 7. Comparison between the experimental drained cyclic test results from Wichtmann [19] and simulations with the HCA model for a stress amplitude variable load history.

Figs. 6 and 7 compare the experimental drained cyclic test results from Wichtmann [19] and simulations with the HCA model for the parameter set listed in Tables 4 and 5 The comparison indicates that the HCA model employed in this paper describes the accumulation of strain for the combinations of deviatoric stress amplitudes (q^{amp}) and average stresses with reasonable accuracy. Here, the average stress represents the average deviatoric stress (q^{av}) and the average mean stress (p^{av}) expected in the FEA. Note that in this comparison, both the HCA and the simple cyclic model – employed to compute the strain amplitude – are evaluated simultaneously; that is, the strain amplitude is not used as a calibration parameter.

3.2.2. Foundation dimensions

The pile considered is a tubular steel pile with an outer diameter $D = 9$m and a constant pile wall thickness $t = 0.08$ m, embedded $L = 36$ m into the soil. This gives a length-to-diameter ratio of $L/D = 4$ and a diameter-to-wall thickness of $D/t = 112.5$, which is representative for monopiles supporting OWTs. For the steel, a Young modulus of $E = 210$ GPa and a Poisson ratio of $\nu = 0.3$ were assumed.

3.3. Numerical modelling aspects

The pile was modelled as a solid volume with an equivalent bending stiffness – which reproduces the bending stiffness of the hollow pile's cross-section, neglecting the stiffness of a soil plug. The suitability of this simplification has been confirmed by Achmus et al. [16]. The cross section of the pile at seabed was modelled as a rigid surface. In each calculation step, loads were applied to the rigid surface and rotation was directly extracted as the updated position of the rigid surface. Pile installation effects were not considered, and the pile was modelled as wished-in-place. Both the geometry and the loading are symmetric around the vertical plane defined by $y = 0$, therefore, it was sufficient to include half of the geometry and the loads in the numerical model.

The mesh had approximately 100000 10-noded tetrahedral soil elements with an average element side length of 2.7 m. The mesh was refined around the pile, where an average element side length of 0.7 m was adopted. The model dimensions were selected in such a way that the accumulation of strains occurred within the model boundaries. Fig. 8 illustrates the dimensions of the finite element model and the mesh refinement. Boundary conditions were applied at the base of the model and at the vertical boundaries. The three displacements components in the three directions were set to zero at bottom boundary. On the vertical boundaries, the normal component was fixed.

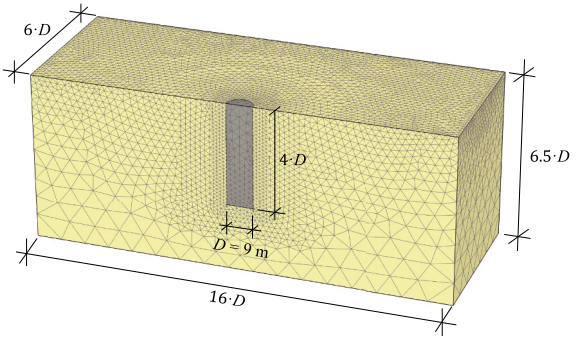

Fig. 8. Finite Element model dimensions and mesh refinement.

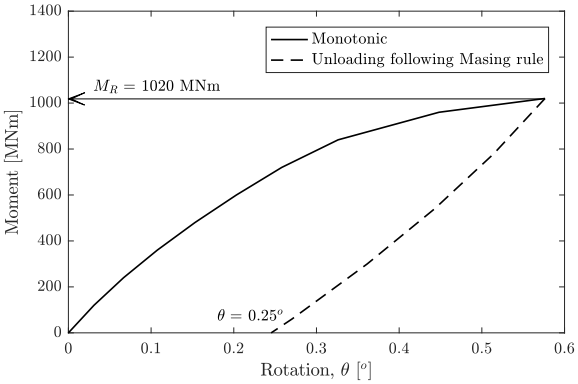

Fig. 9. Definition of the reference moment value, M_R for the WAS-XL monopile.

Table 6
Simulated monopile permanent rotation at the end of each load packet for the ULS storm load history.

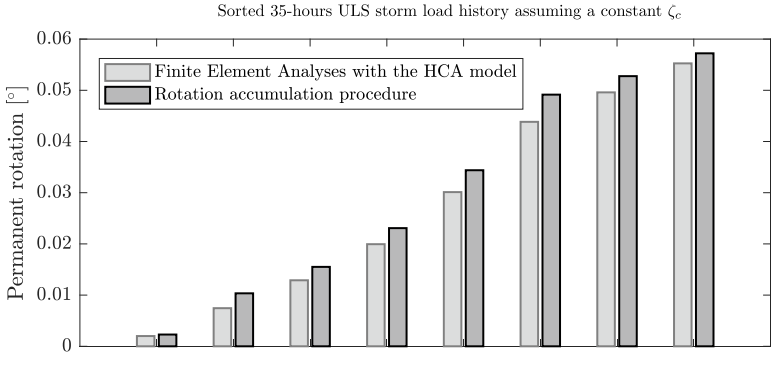

Packet number	1	2	3	4	5	6	7	8
Number of cycles	27748	9413	6340	2560	1055	94	4	1
ζ_c	-0.70	-0.70	-0.70	-0.70	-0.70	-0.70	-0.70	-0.70
ζ_b	0.03	0.09	0.14	0.20	0.28	0.40	0.48	0.57

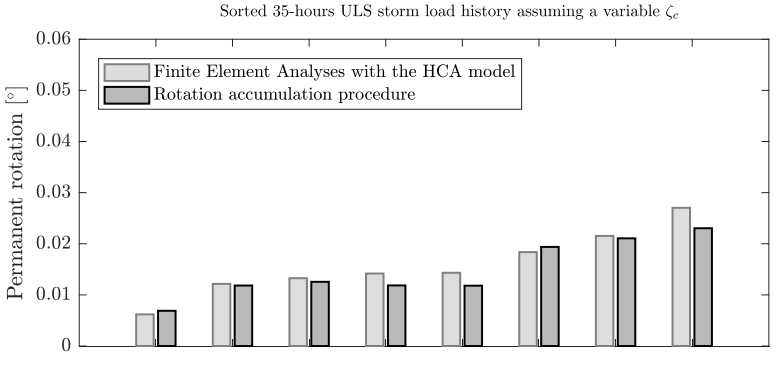

Packet number	1	2	3	4	5	6	7	8
Number of cycles	27748	9413	6340	2560	1055	94	4	1
ζ_c	0.00	-0.51	-0.71	-0.81	-0.88	-0.89	-0.88	-0.85
ζ_b	0.03	0.09	0.14	0.20	0.28	0.40	0.48	0.57

Table 7
Simulated monopile permanent rotation at the end of each load packet for the long-term FLS load history.

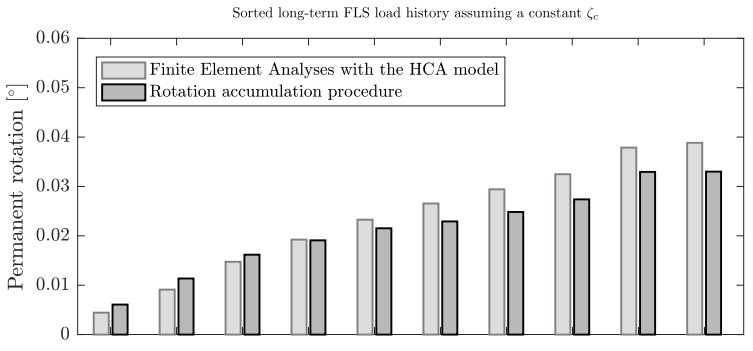

Packet number	1	2	3	4	5	6	7	8	9	10
Number of cycles	10^7	10^7	$8.6 \cdot 10^6$	$2.8 \cdot 10^6$	$1.1 \cdot 10^6$	$2.6 \cdot 10^5$	73400	7292	2211	72
ζ_c	0.0	0.0	0.0	0.0	0.0	0.0	0.0	0.0	0.0	0.0
ζ_b	0.015	0.024	0.035	0.044	0.054	0.064	0.075	0.089	0.113	0.117

3.4. Loading conditions

While design codes provide indications on how to define load histories for ULS (Ultimate Limit State) and FLS (Fatigue Limit State) verifications, there is no clear guidance on how to establish load histories for estimating the permanent rotation for the SLS. Often, designers establish representative SLS load histories from ULS or FLS load histories. In this comparison, the following two series of load histories were considered:

- A load history generated from a 35 h storm sequence for ULS analyses. The loads acting on the monopile foundation were computed from dynamic analyses of the entire OWT based on North Sea hindcast data. For more details on the loads and the hindcast data, the reader is referred to Bachynski et al. [39].
- A load history representative for evaluating the long-term FLS. This load history is generated by combining loads computed from dynamic simulations with: (1) different wind speeds, wave heights, wave periods from North Sea hindcast data, and (2) their probability of occurrence in a 20 year-period. More information on the hindcast data employed to generate the load histories and the probabilities of occurrence can be found in Katsikogiannis [40].

The load histories were extracted from time-domain simulations of the OWT described in Section 3.1. The simulations were carried out in the aero-hydro-servo-elastic software SIMO-RIFLEX from SINTEF Ocean, combined with the multi-directional macro-element model for the soil-structure interaction from Page et al. [41]. The structure was modelled using non-linear beam elements. Aerodynamic loads were applied according to blade element momentum theory, while hydrodynamic loads were computed according to Morison's equation with second order wave kinematics. The load histories were derived assuming that the wind and waves are aligned. The two series of load histories were then sorted out in packets of constant average and cyclic loads and a constant load period by employing rainflow counting. In both, the moment at seafloor in the direction of the wind and wave loading was used as a main load component. A loading arm of 30 m was selected, which corresponded to the water depth, assuming the loads to be mainly wave dominated.

From here, the load characteristics ζ_b and ζ_c were then derived for each packet following Eq. (1). A reference moment value $M_R = 1020$ MN m was selected as the moment that leads to a permanent rotation of 0.25° after an loading-unloading cycle (see Fig. 9), following the criterion proposed by Bayton et al. [26].

Table 8
Physical properties of HST95 silica sand, after [26,42].

Particle size, d_{50}	Specific gravity, G_s	Maximum void ratio, e_{max}	Minimum void ratio, e_{min}	Uniformity coefficient, C_u
[*mm*]	[–]	[–]	[–]	[–]
0.20	2.65	0.827	0.514	1.7

3.5. Results

The comparison between the proposed methodology and 3D FEA of the monopile foundation embedded in a soil volume modelled with the HCA is displayed in Table 6 for the load history representative for a ULS storm, and in Table 7 for the load history representative for long-term FLS analyses. The ULS load history aims at testing the accumulation procedure for relatively high loads applied in a relative limited number of cycles, while the long-term FLS load history aims at testing the procedure for low load levels in combination with a very large number of cycles.

In addition, for the ULS storm load history, the performance of the proposed accumulation procedure is evaluated: (1) assuming a constant ζ_c, corresponding to the average of all load packets, and (2) employing the variable ζ_c derived from the rainflow counting procedure. The case with a constant ζ_c tests the accumulation procedure in a 2D cross-section of the contour diagram (of the type displayed in Fig. 3b), while the case with a variable ζ_c checks the procedure within the full 3D contour space (of the type displayed in Fig. 3c). In the long-term FLS load history, a constant ζ_c, corresponding to the average of all load packets, is assumed.

The comparison indicates that the proposed accumulation procedure can reproduce the results from more advanced 3D FEA within an error of ±15%. It is also worth noting that the permanent rotation is doubled when a constant averaged ζ_c is assumed for the whole load history (Table 6, top), instead of including the actual ζ_c value in each packet (Table 6, bottom).

4. Comparison against centrifuge tests

4.1. Centrifuge experimental set-up

The proposed methodology has also been compared against the experimental results from centrifuge tests documented in Bayton et al. [26]. A series of long-term cyclic lateral load experiments were performed on a geotechnical centrifuge at approximately 100 times Earth's gravity (100*g*), on a fully instrumented model aluminium monopile. The monopile was subjected to an effective stress distribution similar to a monopile with an outer diameter of 5 m, embedded in dense sand to a depth of $L/D = 5$. The sand was a commercially available fine grained sand known as HST95, whose physical properties can be found in Table 8. The model pile was fully instrumented and fabricated from a hollow aluminium section, with a wall thickness scaled to represent the prototype pile flexural stiffness. The sand was pluviated around the monopile as an attempt to model a wished-in-place installation, generating a consistent, constant density sand deposit. Fig. 10 provides a schematic illustration of the centrifuge model setup, with all dimensions noted. Seven centrifuge test were documented in Bayton et al. [26], including:

- One monotonic backbone result. This test provided the reference moment, M_R, estimated as the moment that leads to a permanent rotation upon unload of 0.25°. For the experimental setup, the dimensionless magnitude of $M_R/(\gamma \cdot D^4)$ was equal to 32.7.
- Five single load-amplitude tests were performed with $\zeta_c = 0$ and ζ_b ranging from 0.07 to 0.58. These tests were employed to calibrate some of the soil parameters in the numerical model employed to generate the contour diagrams.
- One multi-amplitude cyclic test whereby packets of successively increasing ζ_b were applied for $\zeta_c = 0$. Seven load packets, ranging from $\zeta_b = 0.04$ to 0.25, of 5000 cycles each were applied, equating to 35000 cycles in total. This last test was employed to compare the prediction from the proposed methodology against experimental results.

4.2. Derivation of contour diagrams

The rotation contour diagram was derived from 3D FEA of the soil and the monopile reproducing the centrifuge test setup described in Section 4.1. Single load-amplitudes – that is, constant ζ_b and ζ_c – were applied. The FEA were performed with the commercial 3D FEA code PLAXIS [38]. The accumulation of strains in the soil, which leads to a monopile accumulated rotation at seafloor, were computed with the HCA model, calibrated based on correlations to physical properties of the sand. Fig. 11 displays the contour diagram computed from FEA.

4.2.1. Estimation of soil parameters for the HCA model

The input parameters in the FEA were either correlated from the physical properties listed in Table 8 or calibrated to fit the experimental results from the single-amplitude centrifuge tests. In particular:

- The HCA model parameters for HST95 sand were derived from the correlations proposed in Wichtmann et al. [29] and listed in Table 9.
- Most of the parameters controlling the cyclic amplitude in Eqs. (3) and (4) were derived from the correlations proposed in Wichtmann and Triantafyllidis[43]. They are listed in Table 10.
- In addition, the parameters g_0 and α from Eq. (3) and the parameter B from Eq. (6) were modified to fit the results from the single-amplitude centrifuge tests, providing the best fit for $g_0 = 800$, $\alpha = 0.75$, and $B = 436$.

Fig. 12 displays the comparison between the permanent rotation measured in the centrifuge tests and the permanent rotation computed from 3D FEA that serves as a basis for the contour diagram. The agreement is good for low values of ζ_b; however it becomes worse as ζ_b increases. This discrepancy is due to the inability of the constitutive model to accurately capture the non-linear permanent

Table 9
Dimensionless parameters of the HCA model for HST95 silica sand estimated from the correlations proposed in Wichtmann et al. [29].

Dimensionless parameter	Correlations from Wichtmann et al. [29]	Value
C_{amp}	$= 1.7$	1.7
C_e	$= 0.95 \cdot e_{min}$	0.488
C_p	$= 0.41 \cdot [1 - 0.34(d_{50} - 0.6)]$	0.466
C_Y	$= 2.60 \cdot [1 + 0.12\ln(d_{50}/0.6)]$	2.257
C_{N1}	$= 4.5 \cdot 10^{-4} \cdot [1 - 0.306\ln(d_{50}/0.6)] \cdot [1 + 3.15(C_u - 1.5)]$	$1.365 \cdot 10^{-3}$
C_{N2}	$= 0.0051\exp[0.39d_{50} + 12.3\exp(-0.77C_u)]$	$9.512 \cdot 10^{-2}$
C_{N3}	$= 1.00 \cdot 10^{-4} \cdot \exp(-0.84d_{50})(C_u - 1.37)^{0.34}$	$6.812 \cdot 10^{-5}$

Table 10
Model parameters employed in the estimation of the strain amplitude for HST95 silica sand, estimated from the correlations proposed in Wichtmann and Triantafyllidis [43] and in Wichtmann and Triantafyllidis [44]. A $p = 50$ kPa and a $p_{atm} = 100$ kPa values are assumed.

Dimensionless parameter	Correlations from literature [43,44]	Value
γ_r	$= \gamma_{r1}(p/p_{atm})^k$	$4 \cdot 10^{-4}$
γ_{r1}	$= 6.2 \cdot 10^{-4}[1 - 0.4(D_{r0} - 0.6)]$	$5.7 \cdot 10^{-4}$
k	$= 0.60 - 0.091\ln(C_u)$	0.54
e_g	$= 1.94\exp(-0.066C_u)$	1.73
n_g	$= 0.40 \cdot C_u^{0.18}$	0.45

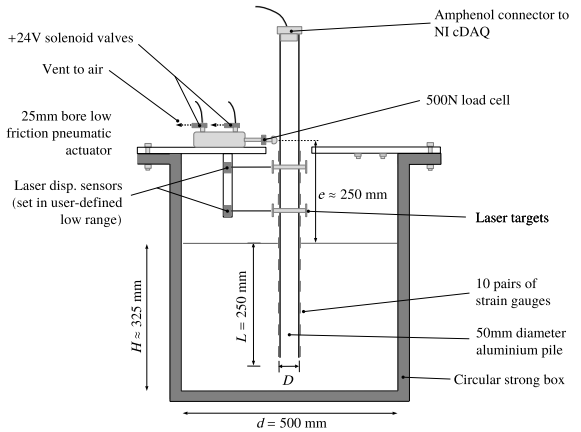

Fig. 10. Centrifuge experimental set-up, modified after [26].

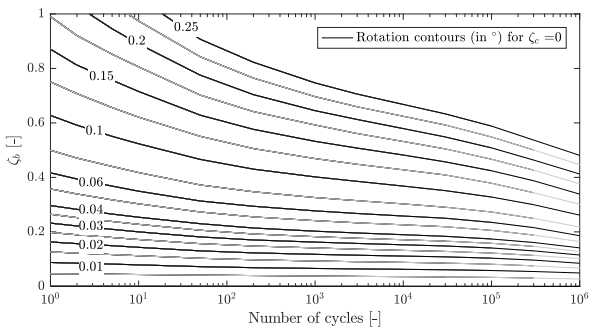

Fig. 11. Contour diagram for the centrifuge model generated from FEA with the HCA model.

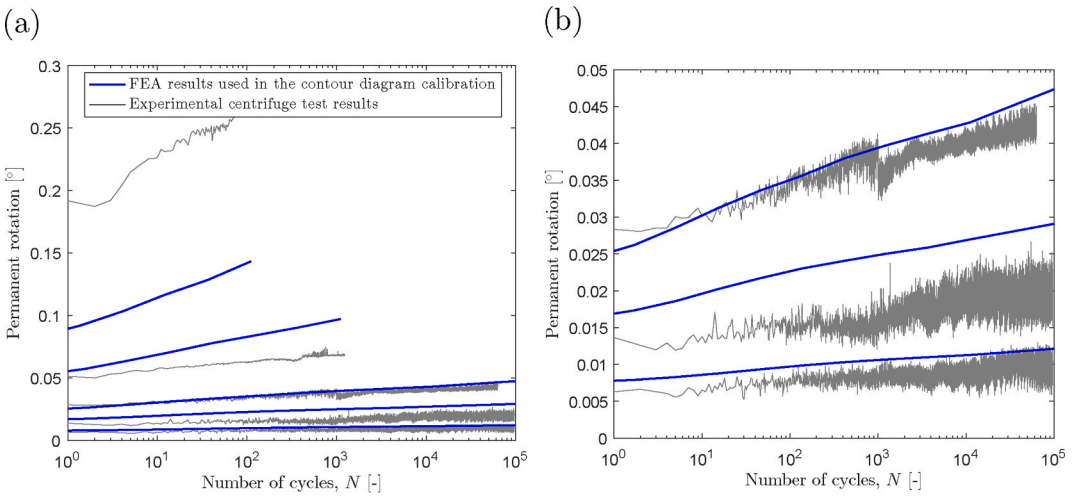

Fig. 12. Comparison between the single-amplitude experimental centrifuge tests from Bayton et al. [26] and the FEA results that serve as a basis for the contour diagram: (a) for $\zeta_b = 0.07$, 0.14, 0.20, 0.39 and 0.58; and (b) zoom in for $\zeta_b = 0.07$, 0.14, and 0.20.

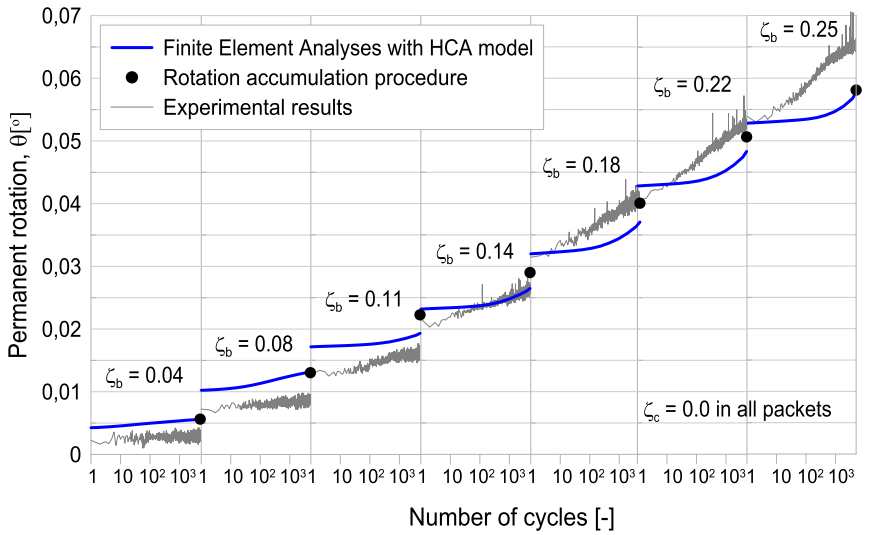

Fig. 13. Comparison between the proposed accumulation procedure, 3D FEA with the HCA model and experimental centrifuge results for a multi-amplitude test.

rotation at $N = 1$ for high ζ_b values.

4.2.2. Finite element model

The Finite Element (FE) model employed to generate the contour diagrams reproduces the centrifuge test setup from Bayton et al. [26] illustrated in Fig. 10. It is based on the following assumptions: only half of the geometry and the loads are included; interface elements with a no-tension criterion are employed between the pile and the soil; fixed boundary conditions are applied at the base and roller boundaries are applied at the lateral boundaries; and the pile is modelled with solid elements with linear elastic properties. The interface stiffness is equivalent to that of the soil, while the interface strength is defined as $\arctan[2/3 \cdot \tan(\varphi_{peak})]$, where φ_{peak} is the peak friction angle of the sand. In addition, the effect of 100*g* gravity in the centrifuge is accounted for in the FE model by a linear increase in the effective unit weight of the sand. A mesh with roughly 100000 soil elements with an average element size of 0.019 m was considered. The mesh was refined around the pile, where an average element length of 0.004 m was employed.

4.3. Results

Fig. 13 displays the comparison between the proposed accumulation procedure and the multi-amplitude centrifuge tests. In addition, Fig. 13 plots results from 3D FEA with the HCA model of the multi-amplitude tests. The comparison indicates that the proposed procedure agrees well with the experimental centrifuge results and with the more advanced 3D FEA. At the end of the multi-amplitude test, the permanent rotation predicted with the proposed procedure matches the permanent rotation computed by more advanced 3D FEA, and deviates from the permanent rotation measured in the experimental centrifuge by 10%. This deviation is mainly due to the differences between the rotation computed in 3D FEA with the HCA model and the measured rotation in the experimental centrifuge tests, which can be attributed to limitations of the constitutive model, inaccuracies in the calibration procedure and measurement imprecision.

5. Discussion

We have presented a methodology to compute the monopile permanent rotation for the SLS under different load histories. The proposed methodology combines an accumulation method with results from 3D FEA. It differs from existing semi-empirical expressions in that the estimated accumulated rotation does not have to be fitted to a pre-defined function and that the calibration is based on drained cyclic triaxial laboratory tests instead of results from pile model tests. The proposed methodology benefits from the accuracy from 3D FEA at the computational speed of simpler methods, as it allows for variations of the load histories without having to repeat computationally expensive FEA.

The proposed procedure has been tested against 3D FEA for a series of ULS and FLS load histories, providing good agreement. This indicates that the use of the permanent rotation as a state variable in the accumulation procedure is reasonable. Using the permanent rotation as state variable implicitly assumes that the soil states – that is, the relative density and stresses – along one contour line are comparable. This assumption seems to be acceptable for the combination of load levels and number of cycles applied in the case study, but it might differ for more extreme combinations.

In addition, the rotation predicted with the proposed procedure has been compared against experimental results from centrifuge tests, providing a reasonable agreement. The deviation between predicted and measured rotation can be attributed to inaccuracies in the numerical model, limitations of the calibration procedure and potential measurement imprecision. With regards to the numerical model, the accuracy of the estimated permanent monopile rotation strongly depends on the ability of the constitutive model to reproduce the accumulated soil strain and its calibration. In this paper, the HCA constitutive model in combination with a simple non-linear elastic cyclic model has been selected, which reproduces the realistic phenomena of accumulation of strains as a function of the number of cycles, relative density and average and cyclic stresses. Despite the HCA capturing most of the realistic phenomena associated to the accumulation of strains, it presents some limitations. First, the model does not always accurately predict the accumulated strain due to variations in the average stress, which might lead to a loss of cyclic memory [45]. In addition, the parameter set is not necessary unique, the flow rule can be too simple for a 3D stress state, and the hardening parameter may not be precise.

The accuracy of the predicted rotation also depends on how realistically the numerical FE model represents the offshore wind farm site conditions, including drainage conditions and installation effects. As indicated in Klinkvort and Page [46] and Li et al. [47], the response of monopiles in sand within a single load cycle might be undrained, and pore pressures might be generated and dissipated in the sand surrounding the monopile. In the examples presented in this paper, we have assumed fully drained conditions and a wished-in-place monopile, which are simplifications of more realistic site conditions. If considered necessary, the effect of drainage can be included in the proposed methodology by generating contour diagrams that incorporate the effect of partial drainage on the accumulated strains. For that purpose, both the HCA [18] or the PDCAM [14] soil models could be employed in the 3D FEA. Installation effects could be included by accounting for changes in the in-situ stresses and void ratio after installation [48]. In addition, the rotation owing to installation could be accounted for by modelling an initially tilted monopile in the FEA.

The proposed methodology presents some limitations that raise questions for future research. One limitation is that the effect of multi-directional loading is not accounted for in the estimation of the permanent rotation. Multi-directional loading could be included by superposition, that is, by defining different radial planes perpendicular to the monopile's cross-section, computing the permanent rotation for the loads acting on each plane, and adding up all the contributions. In addition, results indicate that the predicted rotation is very sensitive to the load characteristic ζ_c, and whether ζ_c is varied or kept constant in the considered load history. Therefore, carrying out more research on the effect of multi-directional loads, and how to select representative ζ_c values is advised.

6. Conclusions

A methodology for estimating the permanent rotation of monopiles for the SLS under different load histories has been developed. The methodology combines results from 3D FEA – with a constitutive model that can account for the accumulation of strains – with an accumulation procedure. It is suitable for this purpose because:

- it predicts the permanent monopile rotation under multi-amplitude load histories observed in experimental centrifuge tests with reasonable accuracy;
- the calibration of the soil response is based on results from cyclic laboratory tests, alone, or in combination with correlations from the literature [29]; which makes the methodology applicable to everyday OWT design;
- it reproduces the permanent monopile rotation computed by time-consuming 3D FEA with reasonable accuracy;

- it is computationally effective. Once the contours are established, different load histories representing the OWT lifetime can be verified at low computational effort. This allows, not only checking different load histories in the design to find out which load history leads to the largest permanent rotation, and therefore is more critical to SLS design, but also understanding the impact of sorting the irregular load histories using different methodologies.

Finally, the results provided in this paper are largely based on numerical simulations. Comparison with laboratory tests (at element level) and field tests and full-scale measurements of OWT (at monopile level) should be carried out to ensure that the numerical results and the assumptions of the proposed methodology – especially the use of the accumulated rotation as state variable – are fair.

Declaration of competing interest

The authors declare that they have no known competing financial interests or personal relationships that could have appeared to influence the work reported in this paper.

Acknowledgements

The authors wish to gratefully acknowledge the financial support by the Research Council of Norway and the industrial partners Equinor, Innogy, EDF, and Multiconsult through the project Wave loads And Soil support for eXtra Large monopiles (WAS-XL), Grant No. 268182, and the financial support received through a NGI internal strategic research project SP9: Behaviour of Sand under Partial Drainage and Offshore Foundation which is funded by the Research Council of Norway through an annual base funding to NGI. In addition, the authors would like to thank: Erin Bachynski and George Katsikogiannis, for providing the verification load histories, and Kristoffer Skjolden Skau and Knut H. Andersen for interesting and fruitful discussions. Centrifuge tests were performed at the Centre for Energy & Infrastructure Ground Research (CEIGR) at the University of Sheffield, UK.

References

[1] Gazzo A, Matzen F, Farhangi C, Lamdaouar A. Offshore wind in Europe - walking the tightrope to success, technical report. Ernst & Young; 2015.
[2] I. R. TCP. Comparative analysis of international offshore wind energy development (REWind offshore), technical report. IEA Renewable Energy Technology Deployment Technology Collaboration Programme (IEA RETD TCP); 2017.
[3] Cuéllar P. Pile foundations for offshore wind turbines: numerical and experimental investigations on the behaviour under short-term and long-term cyclic loading. Ph.D. thesis. Technische Universität Berlin; 2011.
[4] Little RL, Briaud J-L. Full scale cyclic lateral load tests on six single piles in sand, Technical Report. Texas A and M Univ College Station Dept of Civil Engineering; 1988.
[5] Long J, Vanneste G. Effects of cyclic lateral loads on piles in sand. J Geotech Eng 1994;120:225–44.
[6] LeBlanc C, Houlsby G, Byrne B. Response of stiff piles in sand to long-term cyclic lateral loading. Geotechnique 2010;60:79–90.
[7] Klinkvort RT, Hededal O. Lateral response of monopile supporting an offshore wind turbine. Proc Inst Civ Eng Geotech Eng 2013;166:147–58.
[8] Lin S-S, Liao J-C. Permanent strains of piles in sand due to cyclic lateral loads. J Geotech Geoenviron Eng 1999;125:798–802.
[9] Verdure L, Garnier J, Levacher D. Lateral cyclic loading of single piles in sand. Int J Phys Model Geotech 2003;3:17–28.
[10] Peralta P, Achmus M. An experimental investigation of piles in sand subjected to lateral cyclic loads. In: W: Proceedings of 7th international conference on physical modeling in geotechnics, zurich, Switzerland; 2010.
[11] Li Z, Haigh S, Bolton M. Centrifuge modelling of mono-pile under cyclic lateral loads. Phys Model Geotech 2010:965–70.
[12] Dührkop J. Zum Einfluss von Aufweitungen und zyklischen Lasten auf das Verformungsverhalten lateral beanspruchter Pfähle in Sand, Promotionsschrift, Veröffentlichungen des Instituts für Geotechnik und Baubetrieb der TUHH, Bd. 20. Ph.D. thesis, PhD thesis. Hamburg, Germany: University of Technology; 2010.
[13] Bienen B, Dührkop J, Grabe J, Randolph MF, White DJ. Response of piles with wings to monotonic and cyclic lateral loading in sand. J Geotech Geoenviron Eng 2011;138:364–75.
[14] Jostad H, Grimstad G, Andersen K, Saue M, Shin Y, You D. A fe procedure for foundation design of offshore structures–applied to study a potential owt monopile foundation in the Korean western sea. Geotech Eng J SEAGS AGSSEA 2014;45:63–72.
[15] Lesny K, Hinz P, et al. Investigation of monopile behaviour under cyclic lateral loading. In: Offshore site investigation and geotechnics, confronting new challenges and sharing knowledge. Society of Underwater Technology; 2007.
[16] Achmus M, Kuo Y-S, Abdel-Rahman K. Behavior of monopile foundations under cyclic lateral load. Comput Geotech 2009;36:725–35.
[17] Hettler A. Verschiebungen starrer und elastischer Gründungskörper in Sand bei monotoner und zyklischer Belastung, vol. 90. Institut für Bodenmechanik und Felsmechanik der Universität Fridericiana; 1981.
[18] Niemunis A, Wichtmann T, Triantafyllidis T. A high-cycle accumulation model for sand. Comput Geotech 2005;32:245–63.
[19] Wichtmann T. Soil behaviour under cyclic loading: experimental observations, constitutive description and applications. Ph.D. thesis. Institut für Bodenmechanik und Felsmechanik; 2016.
[20] Solf O. Untersuchungen zum mechanischen Verhalten von zyklisch belasteten Offshore-Gründungen. Veröff. Inst. Boden-und Felsmech. Ph.D. thesis, PhD thesis. Karlsruher Institut für Technologie; 2011.
[21] Zachert H. Zur Gebrauchstauglichkeit von Gründungen für Offshore-Windenergieanlagen. Ph.D. thesis. Institut für Bodenmechanik und Felsmechanik am Karlsruher Institut für â€¦; 2015.
[22] Zachert H, Wichtmann T, Triantafyllidis T, Hartwig U. Simulation of a full-scale test on a gravity base foundation for offshore wind turbines using a high cycle accumulation model. In: Frontiers in offshore geotechnics III: proceedings of the 3rd international symposium on frontiers in offshore geotechnics (ISFOG 2015), vol. 1. Taylor & Francis Books Ltd; 2015. p. 819–24.
[23] Li W, Igoe D, Gavin K. Field tests to investigate the cyclic response of monopiles in sand. Proceed Instit Civil Eng Geotech Eng 2015;168:407–21.
[24] LeBlanc C, Byrne B, Houlsby G. Response of stiff piles to random two-way lateral loading. Geotechnique 2010;60:715–21.
[25] Rudolph C, Bienen B, Grabe J. Effect of variation of the loading direction on the displacement accumulation of large-diameter piles under cyclic lateral loading in sand. Can Geotech J 2014;51:1196–206.
[26] Bayton S, Black J, Klinkvort R. Centrifuge modelling of long term cyclic lateral loading on monopiles. In: Physical modelling in geotechnics, ume 1. CRC Press; 2018. p. 689–94.
[27] Truong P, Lehane B, Zania V, Klinkvort RT. Empirical approach based on centrifuge testing for cyclic deformations of laterally loaded piles in sand. Geotechnique 2018;69:133–45.

[28] Andersen K. Behaviour of clay subjected to undrained cyclic loading. Norwegian Geotechnical Institute Publication I; 1976. p. 33–44.
[29] Wichtmann T, Niemunis A, Triantafyllidis T. Improved simplified calibration procedure for a high-cycle accumulation model. Soil Dynam Earthq Eng 2015;70:118–32.
[30] Matsuishi M, Endo T. Fatigue of metals subjected to varying stress, vol. 68. Fukuoka, Japan: Japan Society of Mechanical Engineers; 1968. p. 37–40.
[31] E. ASTM. 1049-85,â€œstandard practices for cycle counting in fatigue analysisâ€. Annu Book ASTM Stand 2005;3:614–20.
[32] Hardin BO, Drnevich VP. Shear modulus and damping in soils: design equations and curves. J Soil Mech Found Div 1972;98.
[33] Hardin BO, Black WL. Sand stiffness under various triaxial stresses. J Soil Mech Found Div 1966;92.
[34] Jostad HP, Dahl BM, Page A, Sivasithamparam N, Sturm H. Evaluation of soil models for improved design of offshore wind turbine foundations in dense sand. Geotechnique 2020:1–18.
[35] Stewart HE. Permanent strains from cyclic variable-amplitude loadings. J Geotech Eng 1986;112:646–60.
[36] Vatne SR. Base case definition for WAS-XL, technical report. SINTEF Ocean AS; 2017.
[37] Velarde J, Bachynski EE. Design and fatigue analysis of monopile foundations to support the DTU 10 MW offshore wind turbine. Energy Procedia 2017;137:3–13.
[38] Brinkgreve R, Kumarswamy S, Swolfs W. PLAXIS 2015. Reference manual. Plaxis bv; 2015.
[39] Bachynski EE, Page AM, Katsikogiannis G. Dynamic response of a large-diamater monopile considering 35-hour storm conditions. In: ASME 2019 38th international conference on ocean, offshore and Arctic engineering. American Society of Mechanical Engineers; 2019.
[40] Katsikogiannis G. Fatigue analysis for unidirectional wind-waves for the DTU 10MW monopile-based offshore wind turbine, , Marinteknisk senter. Norway: Norwegian University of Science and Technology; 2019.
[41] Page AM, Grimstad G, Eiksund GR, Jostad HP. A macro-element model for multidirectional cyclic lateral loading of monopiles in clay. Comput Geotech 2019;106:314–26.
[42] Lauder K. The performance of pipeline ploughs. Ph.D. thesis. UK: University of Dundee Dundee; 2010.
[43] Wichtmann T, Triantafyllidis T. Influence of the grain-size distribution curve of quartz sand on the small strain shear modulus g max. J Geotech Geoenviron Eng 2009;135:1404–18.
[44] Wichtmann T, Triantafyllidis T. Effect of uniformity coefficient on g/g max and damping ratio of uniform to well-graded quartz sands. J Geotech Geoenviron Eng 2012;139:59–72.
[45] Wichtmann T, Triantafyllidis T. Strain accumulation due to packages of cycles with varying amplitude and/or average stress–on the bundling of cycles and the loss of the cyclic preloading memory. Soil Dynam Earthq Eng 2017;101:250–63.
[46] Klinkvort R, Page A. Diameter effect on the lateral response of monopiles in sand supporting offshore wind turbines. 8th European Conference on Numerical Methods in Geotechnical Engineering; 2014.
[47] Li S, Zhang Y, Jostad HP. Drainage conditions around monopiles in sand. Appl Ocean Res 2019;86:111–6.
[48] Engin HK. Modelling pile installation effects: a numerical approach. 2013.